JGR Biogeosciences

RESEARCH ARTICLE
10.1029/2018JG004883

Key Points:
- Sustained nonphotochemical quenching is the major sink for excess light for a high-elevation conifer forest in winter
- A temperature-based acclimation model was able to reproduce seasonal changes in sustained NPQ
- Including a representation of sustained NPQ improved the simulation of SIF for cold-climate evergreens within a land surface model

Supporting Information:
- Supporting Information S1

Correspondence to:
B. Raczka,
Brett.Raczka@utah.edu

Citation:
Raczka, B., Porcar-Castell, A., Magney, T., Lee, J. E., Köhler, P., Frankenberg, C., et al. (2019). Sustained nonphotochemical quenching shapes the seasonal pattern of solar-induced fluorescence at a high-elevation evergreen forest. *Journal of Geophysical Research: Biogeosciences*, *124*, 2005–2020. https://doi.org/10.1029/2018JG004883

Received 19 OCT 2018
Accepted 13 MAY 2019
Accepted article online 29 MAY 2019
Published online 12 JUL 2019

Sustained Nonphotochemical Quenching Shapes the Seasonal Pattern of Solar-Induced Fluorescence at a High-Elevation Evergreen Forest

Brett Raczka[1], A. Porcar-Castell[2], T. Magney[3,4], J. E. Lee[5], P. Köhler[4], C. Frankenberg[3,4], K. Grossmann[6,7,8], B. A. Logan[9], J. Stutz[6,7], P. D. Blanken[10], S. P. Burns[10,11], H. Duarte[12], X. Yang[13], J. C. Lin[12], and D. R. Bowling[1]

[1]School of Biological Sciences, University of Utah, Salt Lake City, UT, USA, [2]Optics of Photosynthesis Laboratory, Institute for Atmospheric and Earth System Research/Forest Sciences, University of Helsinki, Helsinki, Finland, [3]Jet Propulsion Laboratory, California Institute of Technology, Pasadena, CA, USA, [4]Division of Geological and Planetary Sciences, California Institute of Technology, Pasadena, CA, USA, [5]Department of Earth, Environmental and Planetary Sciences, Brown University, Providence, RI, USA, [6]Joint Institute for Regional Earth System Science and Engineering, University of California, Los Angeles, CA, USA, [7]Department of Atmospheric and Oceanic Sciences, University of California, Los Angeles, CA, USA, [8]Institute of Environmental Physics, University of Heidelberg, Heidelberg, Germany, [9]Department of Biology, Bowdoin College, Brunswick, ME, USA, [10]Department of Geography, University of Colorado Boulder, Boulder, CO, USA, [11]National Center for Atmospheric Research, Boulder, CO, USA, [12]Department of Atmospheric Sciences, University of Utah, Salt Lake City, UT, USA, [13]Department of Environmental Sciences, University of Virginia, Charlottesville, VA, USA

Abstract Traditional methods of carbon monitoring in mountainous regions are challenged by complex terrain. Recently, solar-induced fluorescence (SIF) has been found to be an indicator of gross primary production (GPP), and the increased availability of remotely sensed SIF provides an opportunity to estimate GPP across the Western United States. Although the empirical linkage between SIF and GPP is strong, the current mechanistic understanding of this linkage is incomplete and depends upon changes in leaf biochemical processes in which absorbed sunlight leads to photochemistry, heat (via nonphotochemical quenching [NPQ]), fluorescence, or tissue damage. An improved mechanistic understanding is necessary to leverage SIF observations to improve representation of ecosystem processes within land surface models. Here we included an improved fluorescence model within the Community Land Model, Version 4.5 (CLM 4.5), to simulate seasonal changes in SIF at a subalpine forest in Colorado. We found that when the model accounted for sustained NPQ, this provided a larger seasonal change in fluorescence yield leading to simulated SIF that more closely resembled the observed seasonal pattern (Global Ozone Monitoring Experiment-2 [GOME-2] satellite platform and a tower-mounted spectrometer system). We found that an acclimation model based on mean air temperature was a useful predictor for sustained NPQ. Although light intensity was not an important factor for this analysis, it should be considered before applying the sustained NPQ and SIF to other cold climate evergreen biomes. More leaf-level fluorescence measurements are necessary to better understand the seasonal relationship between sustained and reversible components of NPQ and to what extent that influences SIF.

1. Introduction

Monitoring the health of forested ecosystems is important for multiple reasons: their significance for timber resources, watersheds, and the forests' ability to store atmospheric CO_2 as organic material and mitigate current and future climate warming. Globally, land surfaces are responsible for removing 25% of anthropogenic greenhouse gas emissions from the atmosphere, yet it is unclear how much longer the land will maintain that level of ecosystem service (Arora et al., 2013). Within the coterminous United States the eastern third of the nation is primarily forested and provides the majority of carbon uptake (Lu et al., 2015). Perhaps less well recognized is that the Western United States also contributes a significant amount of biomass and carbon uptake (Schimel et al., 2002) and yet is particularly vulnerable to the effects of climate change and disturbance (Williams et al., 2016). This is because the observed (Clow, 2010; Knowles et al., 2006) and projected (Boisvenue & Running, 2010) warming and drying combined with a legacy of fire suppression has increased forest biomass above naturally occurring levels (Houghton et al., 2000; Schimel et al., 2002). This has left the forested regions of the Western United States particularly susceptible to disturbance from insects (Bentz et al., 2010; Hicke et al., 2012), fire (Rocca et al., 2014), and drought-related mortality (Anderegg et al., 2012). Although this warrants continued monitoring, the forests across the Western United States primarily reside in the high-elevation, complex terrain of the Rocky Mountains, a region that is difficult to monitor.

It is challenging to investigate the land-atmosphere carbon exchange across complex terrain using eddy covariance flux towers, terrestrial biosphere modeling, and atmospheric inversions. Flux tower observations are best suited for terrain with homogeneous slope and vegetation, but these conditions are rarely met in mountainous terrain. Terrestrial biosphere models are an effective tool for upscaling large regional fluxes yet include significant uncertainties (Dietze, 2017; Lin et al., 2011) and are difficult to parameterize, especially in terrain that is highly heterogeneous in topography, climate, vegetation, and soil type. Atmospheric inversions are hampered by the limited number of CO_2 observations in the Western United States and complex atmospheric flows induced by the terrain (Lin et al., 2017). The most successful attempts at quantifying carbon fluxes across the Western United States have involved a combination of these approaches, including aircraft observations, but require significant resources (Desai et al., 2011; Sun et al., 2010) that limit the temporal and spatial coverage of carbon flux estimates.

The increasing availability of remotely sensed solar-induced fluorescence (SIF; e.g., Joiner et al., 2014; Köhler et al., 2015) provides an opportunity to improve estimates of carbon uptake across complex terrain. This is because SIF has a strong relationship with gross primary productivity (GPP) across multiple biomes (Alemohammad et al., 2017; Joiner et al., 2014; Sun et al., 2017; Yang et al., 2015), provides a strong constraint for GPP (Koffi et al., 2015; MacBean et al., 2018), and helps identify important mechanisms represented by ecosystem models (Lee et al., 2015; Norton et al., 2018). This is a particularly important development for cold-climate evergreen species prevalent in the Western United States, in which SIF outperforms other greenness or reflectance indices in matching seasonal changes in GPP (Joiner et al., 2014; Magney et al., 2019; Walther et al., 2016; Zuromski et al., 2018). This is because reflectance indices are primarily related to changes in leaf area and leaf color as measured in discrete wave bands that, for boreal or temperate evergreen species, may remain relatively constant across seasonal time scales. Furthermore reflectance indices are susceptible to contamination from ground surface characteristics not representative of the vegetation (Gamon et al., 2013). The SIF, on the other hand, is emitted directly from excited chlorophyll molecules in a process that is linked to photosynthesis, therefore explaining the strong empirical relationship between SIF and GPP for many biomes and time scales (Li et al., 2018; Sun et al., 2017). In some cases, however, the SIF-GPP relationship has been found to be weaker, particularly for crops and evergreen broadleaf forests (Cheng et al., 2013; Yang et al., 2018). Therefore, despite a potentially promising relationship, a more mechanistic understanding is required to leverage SIF observations for improved estimates of GPP and ecosystem processes within terrestrial biosphere models (Porcar-Castell et al., 2014).

When photons are absorbed by chlorophyll, there are three primary pathways for the absorbed energy: (1) photochemistry (photosynthesis), (2) heat dissipation (nonphotochemical quenching [NPQ]), and (3) fluorescence. Chlorophyll molecules and associated structures within the photosystems of plant leaves are responsible for capturing light energy. The light energy is then transported to a reaction center within the photosystem that converts it into chemical energy (electron transport), which is ultimately used to convert atmospheric CO_2 to carbohydrates. In competition with the photochemical transition of energy, a de-excitation reaction that results in the emission of fluorescence occurs. The probability of fluorescence increases with irradiance at low-light conditions and gradually decreases under high-light conditions (Maxwell & Johnson, 2000). To avoid cell damage during periods of excess light, plants have evolved the capacity to dissipate some of this excess energy as heat, via NPQ, primarily through the regulation of xanthophyll cycle pigments (Demmig-Adams & Adams, 2006). For example, a de-epoxidation reaction converts violaxanthin to zeaxanthin, where the zeaxanthin mediates heat dissipation. This increases NPQ (Jahns & Holzwarth, 2012), thereby decreasing the likelihood of photosystem damage. This type of regulation of the xanthophyll cycle occurs relatively quickly (minutes to hours) and reverses during the night and hence is referred to as reversible NPQ (Porcar-Castell, 2011).

An important component of fluorescence models is the empirical relationship between light saturation (fraction of absorbed light not used for photosynthesis) and reversible NPQ (e.g., Flexas et al., 2002). A technique using weak pulse amplitude modulated light that induces active fluorescence emission from plants (PAM fluorometry) has been used for decades to quantify this light saturation-versus-NPQ relationship (Baker, 2008; Porcar-Castell, 2011; van der Tol et al., 2014). Much less research, however, has been devoted to quantifying slower changes in NPQ (e.g., days to months), referred to as sustained NPQ (Demmig-Adams & Adams, 2006; Porcar-Castell, 2011).

Sustained NPQ is an important regulator of light energy for species that maintain leaf area year-round (e.g., temperate, boreal evergreen; Míguez et al., 2015; Porcar-Castell, 2011; Verhoeven, 2014). Unlike the reversible NPQ component, sustained NPQ varies on longer time frames (days, months; Porcar-Castell, 2011) and provides an important outlet for energy during winter dormancy, when photosynthesis is negligible (Bowling et al., 2018; Ensminger et al., 2004). Sustained NPQ is associated with a sustained accumulation of zeaxanthin, but other factors contribute as well (Verhoeven, 2014). Despite this important role, the mechanisms of sustained NPQ are not yet represented in land surface models, and their impact on SIF is unknown. Here we ask: Does sustained NPQ influence the seasonal pattern of SIF for evergreen temperate forests? To that end, we implement a fluorescence submodel within a land surface model (Community Land Model, Version 4.5 [CLM 4.5]) at a high-elevation evergreen forest in the Rocky Mountains of Colorado (Niwot Ridge). We determine whether including a representation of sustained NPQ improves the simulation of the seasonal pattern of SIF by comparing against tower- and satellite-based measurements. In this way we test our mechanistic understanding of the relationship between SIF and GPP, given the empirical relationship between the two (e.g., Sun et al., 2017). This added understanding will improve the ability to use SIF observations to constrain processes that impact the magnitude and pattern of GPP within land surface models.

2. Theory

We provide a theory section that defines the mechanistic representation of fluorescence emission (section 2.1). Next, we give a description of pulse amplitude modulated (PAM) fluorometry measurements that are used to parameterize NPQ (section 2.2). This is followed by the methods (section 3.1) that describe how this representation of fluorescence is implemented within the models. All terms and symbols are defined in Table 1.

2.1. Representation of SIF

The fate of light energy absorbed by a leaf can be represented as the sum of photochemical yield (Φ_P), fluorescence yield (Φ_F), dynamic heat dissipation yield (Φ_N), or basal thermal dissipation yield (Φ_D) as

$$\Phi_P + \Phi_F + \Phi_N + \Phi_D = 1. \tag{1}$$

Whereas Φ_D is the minimum amount of heat lost regardless of leaf chemistry, Φ_N responds to environmental changes on both short (diel) and long (months) time scales. The short, reversible response (Φ_R) represents leaf photoprotection that ramps up during high-light conditions (midday) and the long, sustained response (Φ_S) occurs in response to seasonal changes. This can be expressed as

$$\Phi_N = \Phi_R + \Phi_S. \tag{2}$$

The yields can also be defined in terms of rate coefficients, k, as

$$\Phi_P = k_P/(k_P + k_F + k_N + k_D), \tag{3}$$

$$\Phi_N = k_N/(k_P + k_F + k_N + k_D), \tag{4}$$

$$\Phi_D = k_D/(k_P + k_F + k_N + k_D), \tag{5}$$

$$\Phi_F = k_F/(k_P + k_F + k_N + k_D). \tag{6}$$

Genty et al. (1989) have shown that Φ_F can be related to Φ_P as

Table 1
List of Symbols Used

Symbol	Description	Units
APAR	Absorbed photosynthetically active radiation	$\mu\text{mol}\cdot\text{m}^{-2}\cdot\text{s}^{-1}$
C_i	Leaf intracellular CO_2 partial pressure	Pa
C_p	Leaf CO_2 compensation point	Pa
GPP	Gross primary productivity (canopy photosynthesis)	$\text{g C}\cdot\text{m}^{-2}\cdot\text{day}^{-1}$
F_canopy	Canopy-level emitted fluorescence (radiance)	$\text{W}\cdot\text{m}^{-2}\cdot\mu\text{m}^{-1}\cdot\text{sr}^{-1}$
F_leaf	Leaf-level emitted fluorescence (irradiance)	$\mu\text{mol}\cdot\text{m}^{-2}\cdot\text{s}^{-1}$
F_LNR	Fraction of leaf nitrogen within RuBisCo	$\text{g N}\cdot\text{RuBisCO}\cdot\text{g}^{-1}\text{ N}$
F_m	Maximal dark-acclimated fluorescence (PAM)	$\mu\text{mol}\cdot\text{m}^{-2}\cdot\text{s}^{-1}$
F'_m	Maximal light-acclimated fluorescence (PAM)	$\mu\text{mol}\cdot\text{m}^{-2}\cdot\text{s}^{-1}$
F_mR	Reference, maximal dark-acclimated fluorescence (PAM)	$\mu\text{mol}\cdot\text{m}^{-2}\cdot\text{s}^{-1}$
fnps	Light lost to basal heat dissipation (CLM only)	Fraction
F_t	Instantaneous, light-acclimated fluorescence (PAM)	$\mu\text{mol}\cdot\text{m}^{-2}\cdot\text{s}^{-1}$
F_o	Minimal, dark-acclimated fluorescence (PAM)	$\mu\text{mol}\cdot\text{m}^{-2}\cdot\text{s}^{-1}$
F_v	Difference between F_m and F_o (PAM)	$\mu\text{mol}\cdot\text{m}^{-2}\cdot\text{s}^{-1}$
J_a	Actual electron transport rate	$\mu\text{mol}\cdot\text{m}^{-2}\cdot\text{s}^{-1}$
J_e	Potential electron transport rate	$\mu\text{mol}\cdot\text{m}^{-2}\cdot\text{s}^{-1}$
K	Leaf-to-canopy-level SIF conversion factor	$(\text{W}\cdot\text{m}^{-2}\cdot\mu\text{m}^{-1}\cdot\text{sr}^{-1})(\mu\text{mol}\cdot\text{m}^{-2}\cdot\text{s}^{-1})^{-1}$
k_P	Photochemical rate coefficient	Dimensionless
k_F	Fluorescence rate coefficient	Dimensionless
k_N	Dynamic heat dissipation rate coefficient	Dimensionless
k_D	Basal heat dissipation rate coefficient	Dimensionless
k_R	Reversible, heat dissipation rate coefficient	Dimensionless
k_S	Sustained, heat dissipation rate coefficient	Dimensionless
$k_\text{S,max}$	Seasonal maximum k_S	Dimensionless
NEE	Net ecosystem exchange of carbon	$\text{g C}\cdot\text{m}^{-2}\cdot\text{day}^{-1}$
NPQ	Nonphotochemical quenching (heat dissipation)	Dimensionless
PQ	Photochemical quenching (photosynthesis)	Dimensionless
Φ_P	Photochemical yield	Dimensionless
Φ_Pmax	Maximum, dark-acclimated photochemical yield	Dimensionless
Φ_F	Fluorescence yield	Dimensionless
Φ_N	Dynamic heat dissipation yield	Dimensionless
Φ_D	Dark heat dissipation yield	Dimensionless
Φ_R	Reversible, heat dissipation yield	Dimensionless
Φ_S	Sustained, heat dissipation yield	Dimensionless
psn	Leaf-level photosynthesis	$\mu\text{mol}\cdot\text{m}^{-2}\cdot\text{s}^{-1}$
S	Acclimation state (acclimation model)	°C
SIF	Solar-induced fluorescence	$\text{W}\cdot\text{m}^{-2}\cdot\mu\text{m}^{-1}\cdot\text{sr}^{-1}$
V_cmax	Maximum carboxylation rate at leaf temperature	$\mu\text{mol}\cdot\text{m}^{-2}\cdot\text{s}^{-1}$
x	Degree of light saturation	Fraction
x_CLM	Degree of light saturation calculated with CLM	Fraction
x_PAM	Degree of light saturation calculated with PAM fluorometry	Fraction

Note. For processes related to radiative transfer or heat dissipation, μmol refers to the number of "photons"; for *psn* and V_cmax, μmol refers to the number of CO_2 molecules. Symbols with "PAM" in parentheses are measured with PAM fluorometry. RuBisCo = ribulose-1,5-bisphosphate carboxylase/oxygenase; PAM = pulse amplitude modulated; CLM = Community Land Model.

$$\Phi_\text{F} = \frac{k_\text{F}}{k_\text{F} + k_\text{D} + k_\text{N}}(1-\Phi_\text{P}), \tag{7}$$

where, following van der Tol et al. (2014), $k_\text{F} = 0.05$ and $k_\text{D} = \max(0.03T+0.0773, 0.87)$, where T is temperature in °C. Whereas k_D remains relatively constant, k_N regulates most of the variation in reversible thermal dissipation and is empirically determined through leaf-level measurements using PAM fluorometry (see section 2.2). Φ_P can be expressed in terms of a maximum photochemical yield under dark-acclimated conditions (Φ_Pmax) as

$$\Phi_\text{P} = \Phi_\text{Pmax}(1-x), \tag{8}$$

where x is the degree of light saturation (fraction of absorbed light not used in photosynthesis),

$$x = 1 - \frac{J_a}{J_e}, \tag{9}$$

and J_a and J_e are the actual and potential electron transport rates, respectively. Φ_{Pmax} can be defined in terms of rate coefficients as

$$\Phi_{Pmax} = \frac{k_P}{k_F + k_D + k_P + k_S}, \tag{10}$$

where k_P= 4.0. The traditional definition of Φ_{Pmax} ignores the impact of sustained NPQ such that k_S= 0. In cold-climate evergreen conifers, however, k_S is not negligible; therefore, we have included it in equation (10). The total leaf-level emitted fluorescence (F_{leaf}) is calculated as

$$F_{leaf} = \Phi_F \text{ APAR}, \tag{11}$$

where APAR is the absorbed photosynthetically active radiation.

2.2. PAM Fluorometry

PAM fluorometry measurements are used to define an empirical relationship for the sustained (k_S) and reversible (k_R) components of the NPQ rate coefficients ($k_N = k_R + k_S$; Baker et al., 2008; Porcar-Castell et al., 2014). This method subjects a leaf to saturating pulses of photosynthetically active radiation under light- and dark-acclimated conditions and records the emitted fluorescence. Following Porcar-Castell (2011), the sustained NPQ rate constant is defined as

$$k_S = \left(\frac{F_{mR}}{F_m} - 1\right)(k_F + k_D), \tag{12}$$

where F_m and F_{mR} are the maximal dark-acclimated and reference dark-acclimated maximal fluorescence, respectively. The reference value F_{mR} is the F_m value when sustained NPQ is negligible. This occurs at night, during the growing season. The reversible NPQ rate constant is defined as

$$k_R = \left(\frac{F_{mR}}{F'_m} - \frac{F_{mR}}{F_m}\right)(k_F + k_D), \tag{13}$$

where F'_m is the maximal light-acclimated fluorescence. The reversible NPQ rate coefficient (k_R) responds to the light saturation as measured through PAM fluorometry (x_{PAM}) following van der Tol et al. (2014):

$$x_{PAM} = 1 - \frac{(F'_m - F_t)/F'_m}{(F_m - F_o)/F_m}, \tag{14}$$

where F_t is the light-acclimated steady state fluorescence and F_o is the minimal dark-acclimated fluorescence. The relationship between x_{PAM} and k_R is used to parameterize the relationship within CLM (x_{CLM} versus k_R) that defines k_N (equation (7)). For simplicity, in equations (12) and (13) we assume $k_F + k_D = 1$.

3. Materials and Methods

3.1. Models

We used CLM 4.5 to perform leaf-level fluorescence simulations with three separate model formulations defined as *CLM-SIF*, *CLM-NPQ*, and *CLM-NPQ-k_R(t)*. These formulations primarily differ in the parameterization of k_R and k_S, which we describe in more detail in section 3.5 and in the supporting information (Table S1). CLM provides a fully prognostic description of biogeochemical cycling from the soil subsurface to the top of the vegetation canopy. We used a version of CLM 4.5 that had been previously calibrated to match the carbon, heat, and water exchange characteristics as measured at the AmeriFlux tower (US-NR1) at Niwot Ridge (Raczka et al., 2016). The site-specific calibration included an empirical downscaling of V_{cmax} to accurately simulate the observed seasonal pattern in GPP. Details regarding CLM 4.5 can be found elsewhere (Oleson et al., 2013). Here we emphasize the implementation of the fluorescence submodel within CLM 4.5 that follows the representation used within the Soil Canopy Observation, Photochemistry and Energy fluxes (SCOPE) model, Version 1.7 (van der Tol et al., 2009; van der Tol et al., 2014), a canopy radiation and vegetation model (equations (1)–(11)). The simplifications within CLM 4.5 were based, in part, on a prior implementation of the fluorescence submodel within CLM 4.0 (Lee et al., 2015).

The fluorescence (Φ_F) and photosynthetic yield (Φ_P) follows equations (7) and (8), where k_D=0.95 and

$$\Phi_P = (1-fnps)(1-x_{CLM}), \tag{15}$$

where *fnps* (= 0.15) is the fraction of light lost to basal thermal dissipation and fluorescence in the absence of dynamic heat dissipation (regulatory NPQ). The potential (J_e) and actual (J_a) electron transport rates are defined as

$$J_e = 0.5\,(1-fnps)\ \mathrm{APAR}, \tag{16}$$

$$J_a = 4\,psn\,\frac{C_i + 2C_p}{C_i - C_p}, \tag{17}$$

where *psn* is the nitrogen-limited CO_2 assimilation rate, C_i the leaf intracellular CO_2 concentration, C_p the CO_2 compensation point, and the coefficient 0.5 represents the absorption cross section for photosystem II (PSII). The x_{CLM} is the degree of light saturation calculated with CLM-simulated J_a and J_e. The model formulations *CLM-SIF* and *CLM-NPQ* used an approximation (equations (15) and (16); $\Phi_{Pmax} = 1 - fnps$), whereas *CLM-NPQ-*$k_R(t)$ used equation (10) to define Φ_{Pmax} (Table S1).

CLM 4.5 does not include radiative transfer of fluorescence within the canopy; therefore, similar to Lee et al. (2015), we used the radiative transfer model within SCOPE (van der Tol et al., 2014) to create an empirical conversion factor (K_{740}) as a function of solar zenith angle (SZA) to convert from leaf fluorescence ($\mu mol \cdot m^{-2} \cdot s^{-1}$; equation (11)) to canopy fluorescence ($W \cdot m^{-2} \cdot \mu m^{-1} \cdot sr^{-1}$) at 740 nm and apply this to CLM as

$$F_{canopy} = \frac{F_{leaf}}{K_{740}(\mathrm{SZA})}. \tag{18}$$

SCOPE was also used to generate the complete spectrum of canopy fluorescence radiation that provided a method to convert between radiance values centered upon wave bands that matched the satellite and spectrometer observations (e.g., 740–758 nm). More details of this conversion are provided in the supporting information (Text S1 and Figure S1).

Although we primarily used SCOPE to calculate a leaf-to-canopy level conversion factor (equation (18)) for CLM, SCOPE is also equipped with a representation of leaf biochemistry and photosynthesis. Therefore, we ran a stand-alone version of SCOPE to use as a benchmark against CLM simulations of fluorescence. Unlike CLM, SCOPE does not include a representation of biogeochemical cycling (e.g., dynamic carbon pools); therefore, we prescribed the leaf area index ($4\ m^2\ m^{-2}$), canopy height (13 m), leaf chlorophyll content ($25\ \mu g\ cm^{-2}$; Bowling et al., 2018; Bradford et al., 2008; Burns et al., 2018), and a calibrated seasonally varying V_{cmax} (Raczka et al., 2016) to best match the canopy characteristics and flux observations at US-NR1. We used the same years of meteorological data (1999–2013) from US-NR1 as we used within Raczka et al. (2016).

Ultimately, both CLM and SCOPE simulations matched seasonal changes in observed photosynthesis (Figure S2), an important step for isolating the impact of the fluorescence model formulations. We provide a table of the differences in implementation between CLM and SCOPE fluorescence formulations (Table S1).

3.2. Site: Niwot Ridge, Colorado

We used the subalpine forest site at Niwot Ridge (AmeriFlux: US-NR1) as our focal site because it has clearly distinguishable active and dormant periods for GPP that are strongly related to leaf pigment composition (Bowling et al., 2018; Magney et al., 2019) and likely to influence SIF. We have previous CLM modeling experience at the site (Raczka et al., 2016), and a tower-based spectrometer system (PhotoSpec; section 3.4) was installed in June 2017 to monitor SIF (Grossmann et al., 2018). The US-NR1 site is located in the

Rocky Mountains of Colorado (Burns et al., 2015; Hu et al., 2010; Monson et al., 2002) and consists primarily of temperate evergreen species of lodgepole pine (*Pinus contorta*), Engelmann spruce (*Picea engelmannii*), and subalpine fir (*Abies lasiocarpa*). The forest is approximately 120 years old as a result of forest thinning performed in the early 1900s. Details on the flux measurements, data processing, and quality control are provided in Burns et al. (2015).

3.3. Parameterizing CLM With NPQ Observations

Measurements to quantify seasonality of NPQ were not available at Niwot Ridge; therefore, we used continuous PAM fluorometry measurements from Hyytiälä, Finland, to parameterize the NPQ rate coefficients for the Niwot Ridge model simulations (section 2.2) through a relation with mean air temperature. Seasonal changes in air temperature are known to be a strong determinant of sustained NPQ across a range of biomes (Míguez et al., 2015); therefore, we used the relationship between mean temperature and sustained NPQ measured at Hyytiälä to estimate sustained NPQ changes at Niwot Ridge (section 3.5). Hyytiälä is similar in biome and climate to Niwot Ridge, consisting of a Scots pine (*Pinus sylvestris*) forest that was planted in 1962 after a prescribed burn (Kolari et al., 2009). The fluorescence measurements were made with a MONITORING-PAM Multi-Channel Chlorophyll Fluorometer (MONI-PAM; Porcar-Castell et al., 2008). The fluorescence measurements used in this analysis span from August 2008 through August 2009 (Porcar-Castell, 2011). The temperature record was obtained from the SMEAR II University of Helsinki observation network (Junninen et al., 2009).

3.4. SIF Measurements

We used a tower-mounted scanning spectrometer system (PhotoSpec) installed to evaluate the fluorescence simulations (Grossmann et al., 2018). The PhotoSpec, installed at Niwot Ridge in June 2017, operated continuously between the nadir position (directly down) to ~45° from nadir. The PhotoSpec had a field of view of 0.7° and paused for 20 s in steps of 0.7°. We used 24-hr daily averages of the filtered hourly median values of the PhotoSpec observations in the far-red spectrum (745–758 nm) to estimate a canopy average to compare against our model simulations. The PhotoSpec observations were filtered to remove erroneous values from instrument retrieval errors or nonvegetated surfaces. This included removing data if the photosynthetically active radiation was less than 10 $\mu\text{mol}\cdot\text{m}^{-2}\cdot\text{s}^{-1}$, the normalized difference vegetation index was greater than 0.6, or the far-red SIF retrievals fell within the 1st and 99th percentiles. More details can be found in Grossmann et al. (2018).

We also compared the simulations against a SIF product (Köhler et al., 2015) derived from the Global Ozone Monitoring Experiment-2 (GOME-2) satellite measurements. The satellite soundings used here were filtered for relative cloud fractions < 0.3 and specifically capture the Niwot Ridge location to reduce spatial mismatch. However, the satellite SIF product may have been influenced by land surfaces not representative of the subalpine forest site because of inhomogeneous land cover and coarse spatial resolution of GOME-2 (80×40 km^2 before July 2013 and 40×40 km^2 after). We followed the strategy proposed by Frankenberg et al. (2011) to convert instantaneous SIF measurements to daily, 24-hr averages, which accounts for variations in acquisition time (10:00 am ± 30 min Local Standard Time), length of day, and solar zenith angle. Given the differences in spatial resolution, viewing angle, and daily averaging methodology between the satellite product and PhotoSpec, we expected differences in SIF magnitude but similar relative seasonal changes in SIF. Therefore, we compared relative seasonal changes in SIF between the observations and model simulations.

3.5. Implementation

We provide a summary illustration of the steps required to generate the Niwot Ridge fluorescence simulations (Figure 1). To address the role of sustained NPQ in generating SIF, we performed three separate simulations with CLM: one with a default NPQ parameterization (*CLM-SIF*) that ignored contributions from sustained NPQ, a second with a site-specific NPQ parameterization (*CLM-NPQ*) that accounted for both reversible (k_R) and sustained NPQ (k_S), and a third formulation (*CLM-NPQ-*$k_R(t)$) that is similar to *CLM-NPQ* but includes a seasonally varying representation of reversible NPQ ($k_R(t)$). Following Lee et al. (2015), the *CLM-SIF* simulation used fluorescence data from Flexas et al. (2002) that define a two-parameter fit to represent k_N as

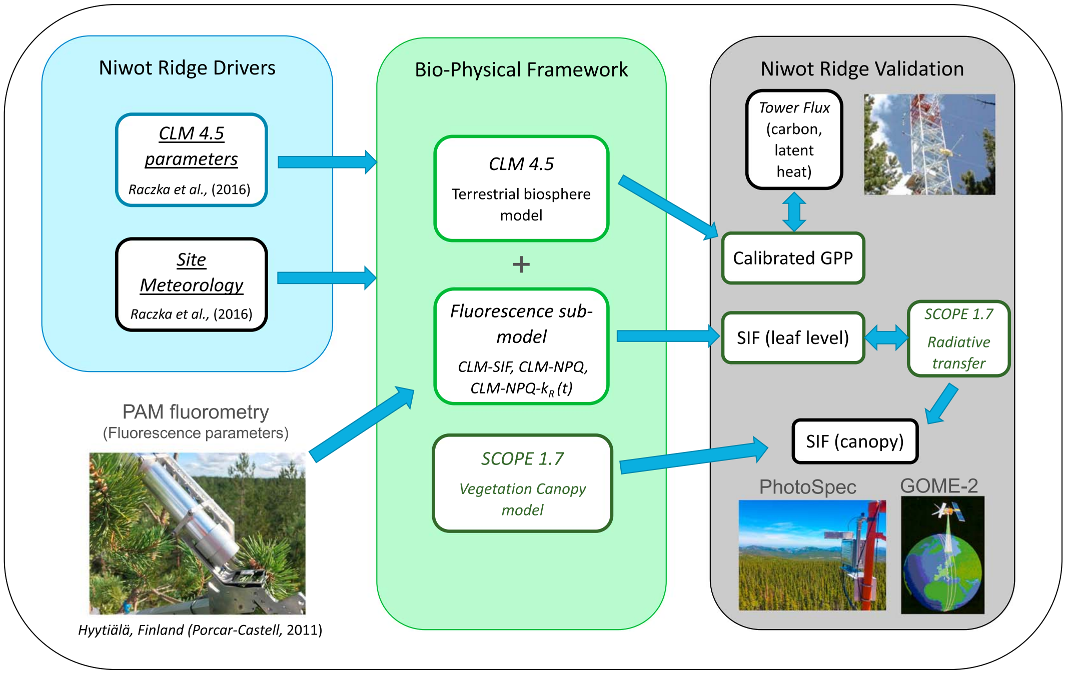

Figure 1. Overview of methodological workflow for model development, calibration, and validation of canopy-level fluorescence at Niwot Ridge. PAM fluorometry measurements were made at Hyytiälä, Finland. Measurements from the tower-mounted PhotoSpec system (Grossmann et al., 2018) and GOME-2 satellite (Köhler et al., 2015) for Niwot Ridge were compared against the CLM 4.5 and SCOPE SIF simulations.

$$k_{\mathrm{N}}(x) = (6.2473x – 0.5944)x. \tag{19}$$

In this formulation $k_{\mathrm{S}} = 0$; therefore, $k_{\mathrm{N}} = k_{\mathrm{R}}$.

CLM-NPQ, on the other hand, parameterized sustained NPQ (k_{S}) independently from reversible NPQ (k_{R}). To estimate k_{S} for Niwot Ridge, we first calculated k_{S} for Hyytiälä (Figure 2). To account for environmental differences (e.g., temperature) between sites (Figure S3) that are known to influence NPQ (Míguez et al., 2015) and phenology (Richardson et al., 2018), we implement an acclimation model designed to simulate phenological changes (e.g., photosynthetic capacity) for cold-climate conifers (Mäkelä et al., 2004). Here we used the daily mean temperature (T) to define an acclimation state (S) as

$$\frac{dS}{dt} = \frac{T – S}{\tau}, \tag{20}$$

where τ determines how quickly S responds to T. Following Kolari et al. (2014), we set $\tau = 7$ days. Given that the transition in sustained NPQ can respond to radiation and photoperiod (Way & Montgomery, 2015), we tested a separate formulation in which incoming shortwave radiation influenced τ such that the response of S was faster under high-light conditions. We also tested a formulation where photoperiod was used as the predictor for sustained NPQ. Including shortwave radiation or photoperiod offered minimal improvement; therefore, for parsimony, we present results only where S was influenced by T. More details concerning the complete range of model formulations tested are provided in the supporting information (Table S2). The acclimation state is used to predict the sustained NPQ (k_{S}) as

$$k_{\mathrm{s}} = \frac{k_{\mathrm{s,\,max}}}{1 + e^{b(S – T_{\mathrm{s}})}} \tag{21}$$

where $k_{\mathrm{s,max}}$ (dimensionless) is the seasonal maximum sustained NPQ and b (°C^{-1}) and Ts (°C) are fitted parameters. We performed separate calibrations for the spring and fall at Hyytiälä (Figure 3) and then applied that relationship to Niwot Ridge using local daily temperature (Figure 4) to obtain the local

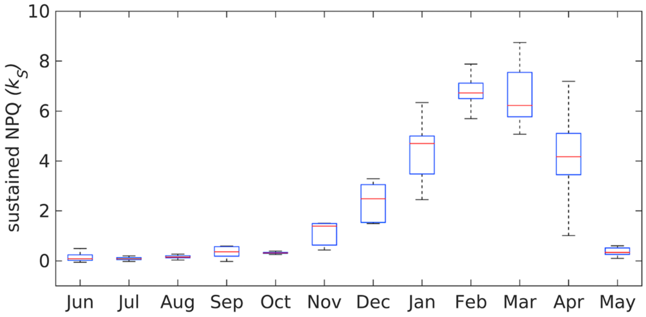

Figure 2. Seasonal pattern in sustained NPQ (k_S) measured in a Scots Pine Forest at Hyytiälä, Finland (2008–2009). Box plots represent the distribution of monthly sustained NPQ calculated for 15-min intervals including the median (red line), interquartile range (blue box), and entire range excluding outliers (black line). The data are from Porcar-Castell (2011).

seasonal pattern in k_S. We inserted that representation of k_S for Niwot Ridge (Figure 4, Niwot Ridge- spring/fall acclimation model) into model formulations *CLM-NPQ and CLM-NPQ-*k_R*(t)* by performing a linear interpolation of k_S between months to provide a smooth seasonal transition. We defined k_R for *CLM-NPQ* by fitting Hyytiälä data to a three-parameter functional form used within the SCOPE model (van der Tol et al., 2014):

$$k_R(x) = k_{no}\,(1+\beta)\,\frac{e^{\alpha\ \ln(x)}}{\beta + e^{\alpha\ \ln(x)}} \tag{22}$$

where $k_{no} = 2.582$, $\beta = 20{,}470$, and $\alpha = 1.043$. This functional form for k_R is illustrated in Figure 5 and labeled *CLM-NPQ*. For *CLM-NPQ-*k_R*(t)*, k_R was fitted to winter and summer data from Hyytiälä (Figure S4). During spring and fall, k_R was transitioned between the winter and summer fits in synchronization with the transition of k_S as modeled at Niwot Ridge (Figure 4).

We performed a final simulation using SCOPE as a benchmark for the CLM fluorescence model development. The SCOPE simulation was similar to the *CLM-SIF* simulation as it used Flexas et al. (2002) data to define a relationship between k_R and x (Figure 5) and ignored k_S (Table S1). We compared the model-simulated canopy fluorescence at Niwot Ridge to measurements from the tower-mounted spectrometer at the site (PhotoSpec; Grossmann et al., 2018) and satellite-inferred fluorescence from measurements from GOME-2 (Köhler et al., 2015). We compared the simulations and observations for a single and multiple years. The years for this comparison were not identical between the simulations and observations; however, we were mainly concerned with seasonal changes in SIF (and GPP), which remained consistent across multiple years.

To quantify the differences between simulated and observed seasonal SIF and k_S, we used piecewise linear regression (Muggeo, 2003, 2008) to define phenological periods (e.g., Magney et al., 2016) using the "segmented" package in R (R Development Core Team, 2018). This software calculates inflection points within the seasonal SIF and NPQ that we used to classify the boundaries of the seasons. The inflection points and the rate of change between the inflection points (slope) were used as metrics for comparison between model simulations and observations.

4. Results

4.1. Sustained and Reversible NPQ

A strong seasonal change in sustained NPQ was observed at Hyytiälä (Figure 2, Table 2, and Figure S5) with the peak monthly average in February (6.71) and minimum monthly average in July (0.09). The widest range (95% CI) of sustained NPQ occurred during the months of January (2.45, 6.35) and April (0.35, 6.76). The transition from low to high sustained NPQ occurred relatively slowly during the fall transition (0.07 unit/day; Table 2 and Figure S5) compared to the transition from high to low sustained NPQ during the spring transition (−0.19 unit/day; Table 2 and Figure S5).

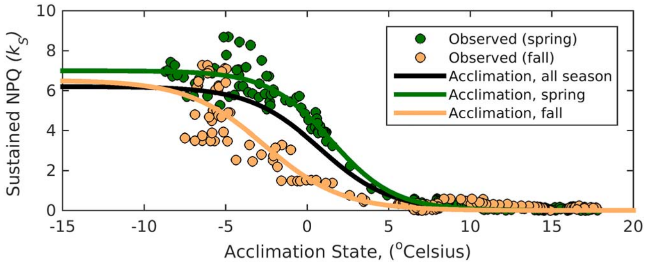

Figure 3. Observed sustained NPQ (k_S; Porcar-Castell, 2011) for Hyytiälä Forest, Finland (years 2008–2009) compared against k_S as simulated from the acclimation model (equations (20) and (21)). The spring/fall acclimation model (R^2: 0.93 RMSE: 0.62) was used to simulate k_S at Niwot Ridge (Figure 4), and the all-season acclimation model (R^2: 0.87 RMSE: 0.98) is shown for reference.

The spring/fall acclimation state model as controlled by daily mean temperature was the best single predictor for sustained NPQ (Figure 3 and Table S2, R^2: 0.93, RMSE: 0.62), whereas the addition of incoming shortwave radiation (R^2: 0.94, RMSE: 0.59) or photoperiod (R^2: 0.90, RMSE: 0.72) provided minimal improvement. Using equation (21), the seasonal pattern of sustained NPQ for Niwot Ridge was similar to the measurements at Hyytiälä with the exception of October through January where lower mean air temperatures at Niwot Ridge (−2.8 and −1.7 °C for each site, respectively) led to calculated sustained NPQ that was higher at Niwot Ridge than measured at Hyytiälä (3.4 and 1.9 for each site, respectively; Figure 4). The acclimation model at Niwot Ridge predicted an early and rapid increase in k_S during the fall transition compared to that at

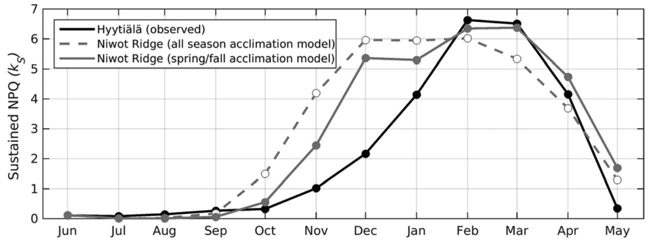

Figure 4. The observed sustained NPQ (k_S) compared against simulated sustained NPQ (k_S) for both Hyytiälä and Niwot Ridge as calculated from the acclimation model (Figure 3). The k_S for Niwot Ridge calculated from the spring/fall acclimation model was inserted into *CLM-NPQ* and *CLM-NPQ-*$k_R(t)$ to account for seasonal changes.

Hyytiälä (Figure 4, Table 2, and Figure S5) with the start and end of the fall transition occurring 30 and 68 days earlier, respectively, for Niwot Ridge. In addition, the acclimation model predicted that the winter season for Niwot Ridge was 62 days longer in duration as compared to that for Hyytiälä.

The reversible NPQ fit based upon all months of the Hyytiälä site data (*CLM-NPQ*; equation (22)) was similar to predictions from the SCOPE model yet much lower than that of the *CLM-SIF* at high-light saturation (equation (19) and Figure 5). Whereas all three functions were similar during relatively low light saturation, for high-light saturation values ($x > 0.6$), the Hyytiälä fit for k_R (*CLM-NPQ*) was on average 43% lower than that of the *CLM-SIF* (Figure 5). This difference in behavior is in part because k_N for *CLM-SIF* is fitted to temperate Mediterranean trees, shrubs, and grapes (Flexas et al., 2002), whereas k_R for *CLM-NPQ* was fitted to the conifer species at Hyytiälä. Although *CLM-NPQ* used a single relationship between reversible NPQ and light saturation (Figure 5), the relationship was found to change with season (Figure S4) and was accounted for in *CLM-NPQ-*$k_R(t)$. In that model formulation the summer k_R (June-August) was on average 2.6 units higher than the winter k_R (January-February) for high-light saturation values ($x > 0.6$).

4.2. Simulated Versus Measured Fluorescence

In general, the CLM simulation that included a representation of sustained NPQ provided a seasonal pattern of SIF more similar to the measurements from the satellite and PhotoSpec (Figure 6, Table 2, and Figure S6). Furthermore the multiyear percent seasonal change in SIF intensity relative to peak values (Figure 6d) was relatively high for *CLM-NPQ* (84%), *CLM-NPQ-*$k_R(t)$ (78%), PhotoSpec (97%), and satellite (~100%), whereas the *CLM-SIF* simulation was lower (70%). This difference in seasonal change in SIF intensity was consistent with changes in fluorescence yield (Φ_F; Figure S2c). The Φ_F seasonal change for *CLM-NPQ* (0.005 to 0.013) and *CLM-NPQ-*$k_R(t)$ (0.005 to 0.012) was greater than that for *CLM-SIF* (0.007 to 0.011). The *CLM-NPQ-*$k_R(t)$ formulation most closely matched the phenological periods as compared to the PhotoSpec observations (Table 2 and Figure S6). For example, the start and duration of the spring transition for *CLM-NPQ-*$k_R(t)$ (start: day of year [doy] 99, duration: 74 days) were nearly identical to those for the PhotoSpec (start: doy 96, duration: 72 days) and significantly outperformed those for *CLM-SIF* (start: doy 19, duration: 150 days).

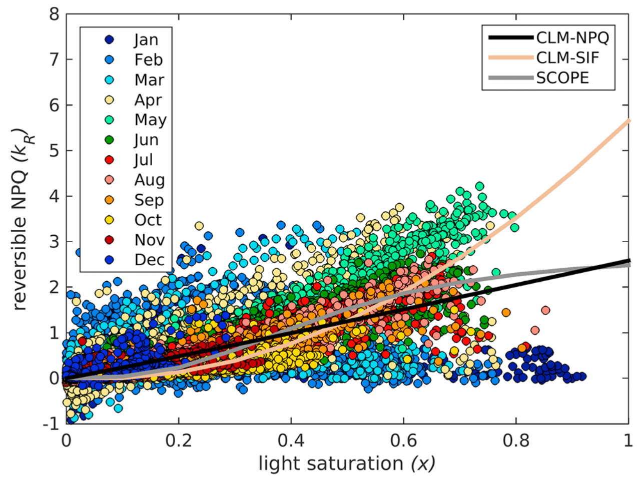

Figure 5. Reversible NPQ (k_R) as calculated from MONI-PAM fluorescence measurements (colored dots) at Hyytiälä (Porcar-Castell, 2011). A single fit for all the data (equation (22)) for the Hyytiälä data was used for the *CLM-NPQ* simulation. *CLM-SIF* and SCOPE simulations used the Flexas et al. (2002) fluorescence data for a two-parameter (equation (19)) and three-parameter fit, respectively, for k_R.

The modeled day-to-day variation in fluorescence (Figure 6a) was higher (in standard deviation: *CLM-SIF*: 0.07 $W \cdot m^{-2} \cdot sr^{-2} \cdot \mu m^{-1}$, *CLM-NPQ*: 0.09 $W \cdot m^{-2} \cdot sr^{-2} \cdot \mu m^{-1}$, *CLM-NPQ-*$k_R(t)$*:* 0.08 $W \cdot m^{-2} \cdot sr^{-2} \cdot \mu m^{-1}$) than the PhotoSpec measurements (0.03 $W \cdot m^{-2} \cdot sr^{-2} \cdot \mu m^{-1}$). However, when normalized by the average magnitude of fluorescence, the percent day-to-day variation was similar between *CLM-SIF* (34%), *CLM-NPQ* (35%), *CLM-NPQ-*$k_R(t)$ (35%), and the PhotoSpec (43%).

5. Discussion

5.1. Impact of Sustained NPQ Upon Seasonal Changes in SIF

Evergreen plants in winter undergo downregulation of photosynthesis with concomitant xanthophyll pigment changes and sustained NPQ (Adams et al., 2004; Verhoeven, 2014), leading to a direct impact on SIF. Here models of SIF that included a representation of seasonal variation of sustained NPQ performed better than those that did not. Including sustained NPQ led to a higher simulated seasonal amplitude and seasonal timing of SIF that were more similar to observations from a tower-mounted spectrometer system and satellite observations. This demonstrates that models must represent seasonal variation in sustained NPQ in order to capture the strong seasonality of SIF in cold-climate evergreens. The importance of seasonal changes in NPQ was consistent with

Table 2
Description of the Phenological Periods From Observed and Simulated SIF ($W\cdot m^{-2}\cdot\mu m^{-1}\cdot sr^{-1}$) and Sustained NPQ (Unitless)

		Spring Transition				Summer				Fall Transition			
Model/Observations	Variable	Start (doy)	End (doy)	Duration (days)	Slope (SIF/day)	Start (doy)	End (doy)	Duration (days)	Slope (SIF/day)	Start (doy)	End (doy)	Duration (days)	Slope (SIF/day)
Photospec (observed)	SIF	96(±1)	168(±1)	72(±1)	2.5e−3	168(±1)	268(±8)	100(±8)	−1.2e−3	268 (±8)	318(±2)	50(±9)	−1.9e−3
CLM-SIF	SIF	19(±2)	169(±1)	150(±2)	1.6e−3	169(±1)	268(±1)	99(±1)	−1.1e−3	268 (±1)	330 (±1)	61(±1)	−2.2e−3
CLM-NPQ	SIF	113(±1)	176(±1)	62(±1)	5.1e−3	176(±1)	265(±1)	89(±1)	−1.4e−3	265(±1)	327(±1)	62(±1)	−4.8e−3
CLM-NPQ-$k_R(t)$	SIF	99(±1)	173(±1)	74(±1)	3.1e−3	173(±1)	268(±1)	95(±1)	−1.3e−3	268(±1)	331(±1)	63(±1)	−3.4e−3

		Fall Transition				Winter				Spring Transition			
		Start (doy)	End (doy)	Duration (days)	Slope (NPQ/day)	Start (doy)	End (doy)	Duration (days)	Slope (NPQ/day)	Start (doy)	End (doy)	Duration (days)	Slope (NPQ/day)
Hyytiälä (observed)	NPQ	329(±4)	43(±4)	79(±6)	7.0e−2	43(±4)	82(±4)	49(±4)	3.0e−3	82(±4)	115(±2)	33(±2)	−1.9e−1
Niwot Ridge Spring/Fall Acclimation Model	NPQ	299(±1)	340(±1)	41(±1)	1.1e−1	340(±1)	86(±1)	111(±1)	1.4e−2	86(±1)	154(±1)	68(±1)	−9.6e−2
Niwot Ridge All Season Acclimation Model	NPQ	274(±1)	338(±1)	64(±1)	9.0e−2	338(±1)	77(±1)	104(±1)	−3.0e−3	77(±1)	154(±1)	77(±1)	−7.4e−2

Note. The start and end dates (day of year [doy]), duration (number of days between start and end dates), and rate of change (slope) for each phenological season were determined by identifying inflection points for seasonal SIF and NPQ (see section 3.5). Seasonal SIF at Niwot Ridge was simulated by the CLM formulations (section 3.5), and the seasonal NPQ for Niwot Ridge was simulated by the acclimation models (section 3.5). The uncertainties (in parentheses) are the standard error of the inflection points. SIF = solar-induced fluorescence; NPQ = nonphotochemical quenching; CLM = Community Land Model.

previous studies at cold-climate conifer forests (Porcar-Castell, 2011; Verhoeven, 2014; Wong & Gamon, 2015; Bowling et al., 2018; Magney et al., 2019) where photoprotection by xanthophyll pigments increased in winter. By linking the sustained NPQ within a fluorescence model, we demonstrated that this increased the seasonal range of Φ_F beyond traditional modeling approaches (e.g., *CLM-SIF* and SCOPE; Figure S2c). This better captured the relative changes in seasonal SIF and improved the timing and rate of transition of SIF during the spring season as observed at Niwot Ridge (Figure S6). Conversely, the omission of sustained NPQ and its influence upon fluorescence will adversely impact parameter optimization studies (e.g., V_{cmax} and chlorophyll content) designed to improve understanding of ecological function (Koffi et al., 2015; Lee et al., 2015; Norton et al., 2018).

In contrast to our results, Thum et al. (2017) provided a reasonable fit to SIF satellite observations using a fluorescence model without explicit representation of seasonally varying sustained NPQ. In that work, the land surface model JSBACH (Reick et al., 2013) was combined with a fluorescence model to provide SIF simulations across four evergreen forest sites in Finland, including Hyytiälä. Whereas our study specifically included a seasonally varying representation of k_S based upon PAM fluorometry, Thum et al. (2017) assumed k_S was 0. In that case k_N was assumed to be controlled by k_R alone and could provide reasonable seasonal changes in NPQ given a single and fixed relationship to light saturation (x). This result could be fortuitous, however, given the large seasonal changes in the x-versus- k_R relationship (Figure S4). Ultimately, distinguishing between k_R and k_S is more realistic and will allow for the appropriate kinetic response at subseasonal times scales for both NPQ and SIF. In addition to differences in the representation of sustained NPQ between Thum et al. (2017) and this analysis, other differences such as the environmental forcing (Figure S3) between the focus sites, and the land surface/fluorescence models (JSBACH versus CLM) may have played a role. To what degree these factors contributed to differences in derived quantities of APAR, Φ_F,and SIF (Figure S2) was beyond the scope of this analysis.

5.2. Daily Mean Temperature as a Predictor of Sustained NPQ

The impact of daily mean temperature upon acclimation state was found to be a strong predictor of sustained NPQ (Figure 3). This relationship between sustained NPQ and temperature at cold-climate evergreen forests is consistent with previous studies (Míguez et al., 2015). The use of temperature to define an acclimation state is consistent with prior work that simulated transitions in photosynthetic capacity at conifer forests (Kolari et al., 2014; Mäkelä et al., 2004) and is similar to the approach in phenology models to determine the timing of budburst and senescence (MacBean et al., 2015; Melaas et al., 2016). Incoming radiation is also known to increase sustained NPQ at cold-climate conifer sites (Ensminger et al., 2004; Porcar-Castell, 2011) and suggests the intersection of high light levels and cold temperatures both influence sustained NPQ. When we included incoming shortwave radiation into sustained NPQ models, the impact was minimal (Table S2). This may have been a result of a limited amount of site

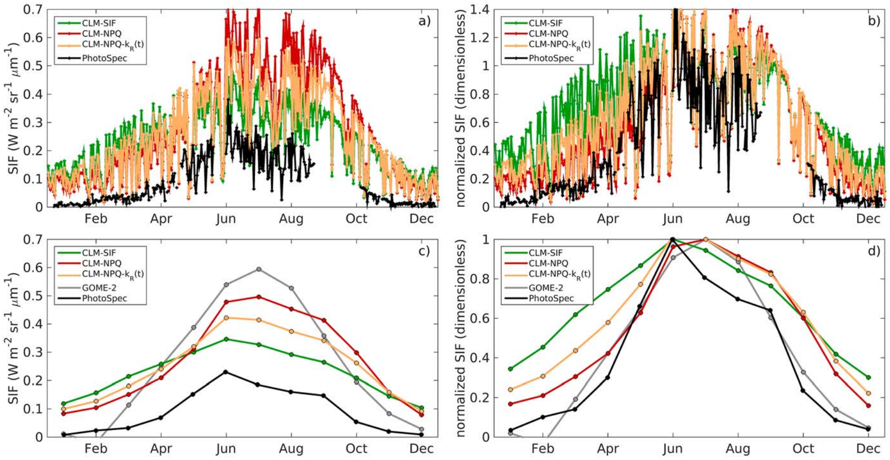

Figure 6. Simulated and observed seasonal patterns of canopy SIF (740 nm) for (a, c) absolute SIF and (b, d) normalized canopy SIF. (a, b) The single-year simulations are in daily resolution for the CLM simulations (year 2010) and PhotoSpec (August 2017 to August 2018). (c, d) The multiyear simulations are monthly averages for the CLM simulations (years 1999–2013), GOME-2 (years 2007–2016), and PhotoSpec (August 2017 to August 2018). The *CLM-SIF* simulation considers reversible NPQ (k_R) only, the *CLM-NPQ* simulation considers both reversible (k_R) and sustained NPQ (k_S), and *CLM-NPQ-*k_R*(t)* considers k_S and seasonal variation in k_R. Both a satellite SIF product (GOME-2; Köhler et al., 2015) and the PhotoSpec measurements (Grossmann et al., 2018) are included for comparison.

data we used for the calibration. Regardless, the intent of this work was to demonstrate the role that sustained NPQ has upon Φ_F and SIF, and temperature alone was sufficient in this regard.

5.3. Impact of Seasonal Variation in Reversible NPQ Upon SIF

All plants protect leaf tissues from excess light via reversible NPQ, mediated by xanthophyll pigments varying in response to incident light (Demmig-Adams & Adams, 2006), yet less is known about how the reversible NPQ varies seasonally. We assumed a fixed relationship for reversible NPQ within our model (i.e., reversible NPQ-versus-light saturation relationship was fixed throughout the year for *CLM-SIF* and *CLM-NPQ*), but the PAM fluorometry data indicated seasonal variation in the magnitude of NPQ as a function of light saturation (Figures 5 and S4). This is consistent with observations of boreal evergreen forests, which have relatively large reversible NPQ responses to light saturation in summer (high incident light) and much smaller but nonzero reversible NPQ response during the winter (low incident light; Porcar-Castell, 2011). When seasonal variation in reversible NPQ (k_R) response was added (*CLM-NPQ-*k_R*(t)*), the comparison with observations improved slightly (Figure 6). For example, the modeled seasonal pattern of monthly SIF increased in correlation for both the satellite (*R*: 0.96 to 0.98) and PhotoSpec (*R*: 0.95 to 0.97). In addition, the *CLM-NPQ-*k_R*(t)* formulation most closely matched the timing of the seasonal transitions as measured by the PhotoSpec (Table S2 and Figure S6). The remaining model-observation mismatch may arise from (1) a deficiency in the acclimation model for k_S that limits its applicability to Niwot Ridge, (2) a unique behavior in k_R across site and conifer species, or (3) limitations of the fluorescence model within CLM. The fact that all model formulations predicted significant SIF throughout the winter, where observations fell to near zero, suggests that Φ_F was overestimated in the winter. This could mean either that the assumption of a constant PSII absorption cross section was too simplistic (Equation (16)) or that an explicit representation of the deactivation of PSII reaction centers was required. Overall, more research that combines site-level measurements of SIF, k_R, and k_S at Niwot Ridge in particular is needed to better understand the cause of the model-observation mismatch.

5.4. Recommendations for Future SIF Modeling Improvements

We have used PAM fluorometry measurements to improve SIF modeling within CLM 4.5 by adding seasonal changes in NPQ at a high-elevation forest site. An opportunity remains to use fluorometry measurements to also define seasonal changes in photochemical yield. The photochemical yield in CLM presented here is imposed through the Farquhar et al. (1980) photosynthesis model (V_{cmax} and J_{max}).

Seasonal changes in photosynthetic activity are represented by adjusting V_{cmax} in the winter months through leaf temperature (Arrhenius equation) and a day length factor (Oleson et al., 2013). In practice, these factors alone cannot properly simulate seasonal changes in GPP (photosynthetic yield), requiring an additional empirical adjustment (Raczka et al., 2016). As a result, the seasonal variation of photochemical yield (determined through V_{cmax} and J_{max}) and the fluorescence model (equation (15)) are weakly linked, and there remains an opportunity to unify the model for internal consistency. For example, the seasonal variation in sustained NPQ (Figure 2) could help define the day length factor, improving the seasonal behavior of the leaf energy balance. Also, the photochemical yield as estimated through the fluorescence measurements could be used as an independent means to check the parameter values within the existing V_{cmax} parameterization.

Although we have included reversible and sustained components of NPQ and demonstrated their influence upon SIF, there are other potentially important processes that are not represented in CLM. Seasonal changes in chlorophyll concentration may also influence APAR and the NPQ/PQ characteristics. Although chlorophyll concentration remains fairly constant throughout the year at Niwot Ridge (Bowling et al., 2018), this is not always the case for other cold-climate evergreen forests (Ensminger et al., 2004; Porcar-Castell et al., 2012; Wong & Gamon, 2015). Furthermore, low-latitude sites such as Niwot Ridge are exposed to increased amounts of excess light (relative to high latitudes) during the winter months, which could increase the level of photoinhibition for the photochemical reaction centers. Similarly to NPQ, a proxy for the fraction of active and functional reaction centers can be derived through PAM fluorometry (Porcar-Castell et al., 2014). A fluorescence model with explicit representation of both NPQ and functional reaction centers (developed by Federico Magnani) has been implemented in SCOPE and JSBACH but not yet tested. The lack of representation of functional reaction centers could account for some of the SIF mismatch between the CLM model formulations and observations (Figures 6 and S7).

We performed an independent, calibrated simulation of SCOPE to provide a leaf-to-canopy SIF conversion factor (K) for CLM. This was necessary because the implementation of CLM did not include within-canopy SIF radiative transfer. This approach was feasible for a single-site simulation, but challenges arise for a larger spatial domain where the conversion factor is a function of canopy characteristics. Canopy radiative transfer depends upon multiple features (e.g., vegetation structure, leaf pigment content, and sun angle) that can vary significantly by location. It is possible to empirically define a leaf-to-canopy SIF conversion factor based upon a subset of canopy characteristics (Lee et al., 2015), but ultimately including a better representation of canopy radiative transfer to dynamically convert leaf-to-canopy level SIF within CLM is a more practical, long-term solution. Such radiative transfer schemes have been included in other land surface models (Thum et al., 2017). Ultimately, including that level of radiative detail within a global Earth system model will substantially increase the computational costs, and implementation should be weighed against the available resources.

6. Conclusions

We have included a representation of sustained NPQ within CLM 4.5, equipped with a SIF model, and have performed a simulation at a high-elevation evergreen forest within the U.S. Rocky Mountains. When the seasonality of NPQ was calculated using leaf-level fluorescence measurements, the simulated seasonal variation in SIF more closely matched satellite- and tower-based SIF observations. This suggests that seasonality of NPQ is an important influence upon SIF for middle- and high-latitude evergreen forests that experience strong seasonal temperature change. Attempts to use SIF observations to constrain photosynthetic processes/parameterization without representation of seasonality in NPQ will lead to biased results. Despite our improvements, all of the SIF formulations implemented into CLM tended to underestimate percent changes in SIF and overestimated SIF in the winter. More measurements are necessary to understand whether this mismatch can be resolved with improved NPQ parameterizations specifically or through more mechanistic SIF modeling approaches overall. The strong linkage between air temperature and sustained NPQ provides confidence that air temperature may be used as a first-order predictor of sustained NPQ. Although including light level did not significantly improve the prediction of NPQ in this case, we anticipate light levels will be an important predictor if the proposed model for sustained NPQ is applied across a wider region. This is significant because continuous PAM fluorometry measurements used to calibrate sustained

NPQ are rare, and simple approaches to estimate NPQ from environmental forcing would be valuable for Earth system modeling.

Acknowledgments
This research was supported by the NASA CMS Project (award NNX16AP33G) and the U.S. Department of Energy's Office of Science, Terrestrial Ecosystem Science Program (awards DE-SC0010624 and DE-SC0010625). CESM is sponsored by the National Science Foundation and the U.S. Department of Energy. Funding for the AmeriFlux core site data (US-NR1/Niwot Ridge, PI: Peter Blanken) was provided by the U.S. DOE Office of Science through the AmeriFlux Management Project at Lawrence Berkeley National Laboratory under award 7094866. A. P. C. was supported by the Academy of Finland (grant 288039). Thank you to Christian van der Tol for making the SCOPE model freely available and for helpful discussion. We also thank Nick Parazoo, Mingjie Shi, and Anna Trugman for helpful discussion during the development of this manuscript. We would like to thank the Center for High Performance Computing at the University of Utah. We used AmeriFlux data provided for Niwot Ridge (Blanken et al., 2018) to perform the CLM and SCOPE simulations. Temperature data from Hyytiälä, Finland, were from the SMEAR II University of Helsinki observation network (Junninen et al., 2009). SIF satellite data were from Köhler et al. (2015), and PhotoSpec data from Grossmann et al. (2018). The model code for SCOPE and CLM can be downloaded from https://github.com/Christiaanvandertol/SCOPE and https://github.com/ESCOMP/ctsm.git, respectively. The source code for the specific CLM model formulations used in this manuscript is located at https://github.com/bmraczka/sustained_NPQ.

References

Adams, W. W., Zarter, C. R., Ebbert, V., & Demmig-Adams, B. (2004). Photoprotective strategies of overwintering evergreens. *BioScience*, *54*(1), 41–49. https://doi.org/10.1641/0006-3568(2004)054[0041:PSOOE]2.0.CO;2

Alemohammad, S. H., Fang, B., Konings, A. G., Aires, F., Green, J. K., Kolassa, J., et al. (2017). Water, Energy, and Carbon with Artificial Neural Networks (WECANN): A statistically based estimate of global surface turbulent fluxes and gross primary productivity using solar-induced fluorescence. *Biogeosciences*, *14*(18), 4101–4124. https://doi.org/10.5194/bg-14-4101-2017

Anderegg, W. R. L., Berry, J. A., Smith, D. D., Sperry, J. S., Anderegg, L. D. L., & Field, C. B. (2012). The roles of hydraulic and carbon stress in a widespread climate-induced forest die-off. *Proceedings of the National Academy of Sciences of the United States of America*, *109*(1), 233–237. https://doi.org/10.1073/pnas.1107891109

Arora, V. K., Boer, G. J., Friedlingstein, P., Eby, M., Jones, C. D., Christian, J. R., et al. (2013). Carbon-concentration and carbon-climate feedbacks in CMIP5 Earth system models. *Journal of Climate*, *26*(15), 5289–5314. https://doi.org/10.1175/jcli-d-12-00494.1

Baker, N. R. (2008). Chlorophyll fluorescence: A probe of photosynthesis in vivo. *Annual Review of Plant Biology*, *59*(1), 89–113. https://doi.org/10.1146/annurev.arplant.59.032607.092759

Bentz, B. J., Régnière, J., Fettig, C. J., Hansen, E. M., Hayes, J. L., Hicke, J. A., et al. (2010). Climate change and bark beetles of the Western United States and Canada: Direct and indirect effects. *BioScience*, *60*(8), 602–613. https://doi.org/10.1525/bio.2010.60.8.6

Blanken, P. D., Monson, R. K., Burns, S. P., Bowling, D. R., & Turnipseed, A. A. (2018). Data and information for the AmeriFlux US-NR1 Niwot Ridge Subalpine Forest (LTER NWT1) site. *AmeriFlux Mangement Project, Berkeley, CA: Lawrence Berkeley National Laboratory.*. https://doi.org/10.17190/AMF/1246088

Boisvenue, C., & Running, S. W. (2010). Simulations show decreasing carbon stocks and potential for carbon emissions in Rocky Mountain forests over the next century. *Ecological Applications*, *20*(5), 1302–1319. https://doi.org/10.1890/09-0504.1

Bowling, D. R., Logan, B. A., Hufkens, K., Aubrecht, D. M., Richardson, A. D., Burns, S. P., et al. (2018). Limitations to winter and spring photosynthesis of a Rocky Mountain subalpine forest. *Agricultural and Forest Meteorology*, *252*, 241–255. https://doi.org/10.1016/j.agrformet.2018.01.025

Bradford, J. B., Birdsey, R. A., Joyce, L. A., & Ryan, M. G. (2008). Tree age, disturbance history, and carbon stocks and fluxes in subalpine Rocky Mountain forests. *Global Change Biology*, *14*(12), 2882–2897. https://doi.org/10.1111/j.1365-2486.2008.01686.x

Burns, S. P., Blanken, P. D., Turnipseed, A. A., Hu, J., & Monson, R. K. (2015). The influence of warm-season precipitation on the diel cycle of the surface energy balance and carbon dioxide at a Colorado subalpine forest site. *Biogeosciences*, *12*(23), 7349–7377. https://doi.org/10.5194/bg-12-7349-2015

Burns, S. P., Swenson, S. C., Wieder, W. R., Lawrence, D. M., Bonan, G. B., Knowles, J. F., & Blanken, P. D. (2018). A comparison of the diel cycle of modeled and measured latent heat flux during the warm season in a Colorado subalpine forest. *Journal of Advances in Modeling Earth Systems*, *10*(3), 617–651. https://doi.org/10.1002/2017MS001248

Cheng, Y.-B., Middleton, E. M., Zhang, Q., Huemmrich, K. F., Campbell, P. K. E., Cook, B., et al. (2013). Integrating solar induced fluorescence and the photochemical reflectance index for estimating gross primary production in a cornfield. *Remote Sensing*, *5*(12), 6857–6879. https://doi.org/10.3390/rs5126857

Clow, D. W. (2010). Changes in the timing of snowmelt and streamflow in Colorado: A response to recent warming. *Journal of Climate*, *23*(9), 2293–2306. https://doi.org/10.1175/2009JCLI2951.1

Demmig-Adams, B., & Adams, W. W. (2006). Photoprotection in an ecological context: The remarkable complexity of thermal energy dissipation. *New Phytologist*, *172*(1), 11–21. https://doi.org/10.1111/j.1469-8137.2006.01835.x

Desai, A. R., Moore, D. J., Ahue, W. K., Wilkes, P. T., De Wekker, S. F., Brooks, B. G., et al. (2011). Seasonal pattern of regional carbon balance in the central Rocky Mountains from surface and airborne measurements. *Journal of Geophysical Research*, *116*(4), G04009. https://doi.org/10.1029/2011JG001655

Dietze, M. C. (2017). Prediction in ecology: A first-principles framework. *Ecological Applications*, *27*(7), 2048–2060. https://doi.org/10.1002/eap.1589

Ensminger, I., Sveshnikov, D., Campbell, D. A., Funk, C., Jansson, S., Lloyd, J., et al. (2004). Intermittent low temperatures constrain spring recovery of photosynthesis in boreal Scots pine forests. *Global Change Biology*, *10*(6), 995–1008. https://doi.org/10.1111/j.1365-2486.2004.00781.x

Farquhar, G. D., von Caemmerer, S., & Berry, J. A. (1980). A biochemical model of photosynthetic CO_2 assimilation in leaves of C_3 species. *Planta*, *149*(1), 78–90. https://doi.org/10.1007/BF00386231

Flexas, J., Escalona, J. M., Evain, S., Gulías, J., Moya, I., Osmond, C. B., & Medrano, H. (2002). Steady-state chlorophyll fluorescence (Fs) measurements as a tool to follow variations of net CO_2 assimilation and stomatal conductance during water-stress in C_3 plants. *Physiologia Plantarum*, *114*(2), 231–240. https://doi.org/10.1034/j.1399-3054.2002.1140209.x

Frankenberg, C., Fisher, J. B., Worden, J., Badgley, G., Saatchi, S. S., Lee, J.-E., et al. (2011). New global observations of the terrestrial carbon cycle from GOSAT: Patterns of plant fluorescence with gross primary productivity. *Geophysical Research Letters*, *38*, L17706. https://doi.org/10.1029/2011GL048738

Gamon, J. A., Huemmrich, K. F., Stone, R. S., & Tweedie, C. E. (2013). Spatial and temporal variation in primary productivity (NDVI) of coastal Alaskan tundra: Decreased vegetation growth following earlier snowmelt. *Remote Sensing of Environment*, *129*, 144–153. https://doi.org/10.1016/j.rse.2012.10.030

Grossmann, K., Frankenberg, C., Magney, T. S., Hurlock, S. C., Seibt, U., & Stutz, J. (2018). PhotoSpec: A new instrument to measure spatially distributed red and far-red solar-induced chlorophyll fluorescence. *Remote Sensing of Environment*, *216*, 311–327. https://doi.org/10.1016/j.rse.2018.07.002

Hicke, J. A., Allen, C. D., Desai, A. R., Dietze, M. C., Hall, R. J., , Ted Hogg E. H., et al. (2012). Effects of biotic disturbances on forest carbon cycling in the United States and Canada. *Global Change Biology*, *18*(1), 7–34. https://doi.org/10.1111/j.1365-2486.2011.02543.x

Houghton, R. A., Hackler, J. L., & Lawrence, K. T. (2000). Changes in terrestrial carbon storage in the United States. 2: The role of fire and fire management. *Global Ecology and Biogeography*, *9*(2), 145–170. https://doi.org/10.1046/j.1365-2699.2000.00164.x

Hu, J., Moore, D. J. P., Burns, S. P., & Monson, R. K. (2010). Longer growing seasons lead to less carbon sequestration by a subalpine forest. *Global Change Biology*, *16*(2), 771–783. https://doi.org/10.1111/j.1365-2486.2009.01967.x

Jahns, P., & Holzwarth, A. R. (2012). The role of the xanthophyll cycle and of lutein in photoprotection of photosystem II. *Biochimica et Biophysica Acta (BBA) - Bioenergetics*, *1817*(1), 182–193. https://doi.org/10.1016/j.bbabio.2011.04.012

Joiner, J., Yoshida, Y., Vasilkov, A. P., Schaefer, K., Jung, M., Guanter, L., et al. (2014). The seasonal cycle of satellite chlorophyll fluorescence observations and its relationship to vegetation phenology and ecosystem atmosphere carbon exchange. *Remote Sensing of Environment*, *152*, 375–391. https://doi.org/10.1016/j.rse.2014.06.022

Junninen, H., Lauri, A., Keronen, P., Aalto, P., Hiltunen, V., Hari, P., & Kulmala, M. (2009). Smart-SMEAR: On-line data exploration and visualization tool for SMEAR stations. Retrieved from https://helda.helsinki.fi/handle/10138/233466

Knowles, N., Dettinger, M. D., & Cayan, D. R. (2006). Trends in snowfall versus rainfall in the Western United States. *Journal of Climate*, *19*(18), 4545–4559. https://doi.org/10.1175/JCLI3850.1

Koffi, E. N., Rayner, P. J., Norton, A. J., Frankenberg, C., & Scholze, M. (2015). Investigating the usefulness of satellite-derived fluorescence data in inferring gross primary productivity within the carbon cycle data assimilation system. *Biogeosciences*, *12*(13), 4067–4084. https://doi.org/10.5194/bg-12-4067-2015

Köhler, P., Guanter, L., & Joiner, J. (2015). A linear method for the retrieval of sun-induced chlorophyll fluorescence from GOME-2 and SCIAMACHY data. *Atmos. Meas. Tech.*, *8*(6), 2589–2608. https://doi.org/10.5194/amt-8-2589-2015

Kolari, P., Chan, T., Porcar-Castell, A., Bäck, J., Nikinmaa, E., & Juurola, E. (2014). Field and controlled environment measurements show strong seasonal acclimation in photosynthesis and respiration potential in boreal Scots pine. *Functional Plant Ecology*, *5*(717). https://doi.org/10.3389/fpls.2014.00717

Kolari, P., Kulmala, L., Pumpanen, J., Launiainen, S., Ilvesniemi, H., Hari, P., & Nikinmaa, E. (2009). CO_2 exchange and component CO_2 fluxes of a boreal Scots pine forest. Retrieved from https://helda.helsinki.fi/handle/10138/233561

Lee, J.-E., Berry, J. A., van der Tol, C., Yang, X., Guanter, L., Damm, A., et al. (2015). Simulations of chlorophyll fluorescence incorporated into the Community Land Model version 4. *Global Change Biology*, *21*(9), 3469–3477. https://doi.org/10.1111/gcb.12948

Li, X., Xiao, J., He, B., Altaf Arain, M., Beringer, J., Desai, A. R., et al. (2018). Solar-induced chlorophyll fluorescence is strongly correlated with terrestrial photosynthesis for a wide variety of biomes: First global analysis based on OCO-2 and flux tower observations. *Global Change Biology*, *24*(9), 3990–4008. https://doi.org/10.1111/gcb.14297

Lin, J. C., Mallia, D. V., Wu, D., & Stephens, B. B. (2017). How can mountaintop CO_2 observations be used to constrain regional carbon fluxes? *Atmos. Chem. Phys.*, *17*(9), 5561–5581. https://doi.org/10.5194/acp-17-5561-2017

Lin, J. C., Pejam, M. R., Chan, E., Wofsy, S. C., Gottlieb, E. W., Margolis, H. A., & McCaughey, J. H. (2011). Attributing uncertainties in simulated biospheric carbon fluxes to different error sources. *Global Biogeochemical Cycles*, *25*, GB2018. https://doi.org/10.1029/2010GB003884

Lu, X., Kicklighter, D. W., Melillo, J. M., Reilly, J. M., & Xu, L. (2015). Land carbon sequestration within the conterminous United States: Regional- and state-level analyses. *Journal of Geophysical Research: Biogeosciences*, *120*, 379–398. https://doi.org/10.1002/2014JG002818

MacBean, N., Maignan, F., Peylin, P., Bacour, C., Bréon, F.-M., & Ciais, P. (2015). Using satellite data to improve the leaf phenology of a global terrestrial biosphere model. *Biogeosciences*, *12*(23), 7185–7208. https://doi.org/10.5194/bg-12-7185-2015

MacBean, N., Maignan, F., Bacour, C., Lewis, P., Peylin, P., Guanter, L., et al. (2018). Strong constraint on modelled global carbon uptake using solar-induced chlorophyll fluorescence data. *Scientific Reports*, *8*(1), 1973. https://doi.org/10.1038/s41598-018-20024-w

Magney, T. S., Bowling, D. R., Logan, B. A., Grossmann, K., Stutz, J., Blanken, P. D., et al. (2019). Mechanistic evidence for tracking the seasonality of photosynthesis with solar-induced fluorescence. *Proceedings of the National Academy of Sciences of the United States of America*, *116*(24), 11,640–11,645. https://doi.org/10.1073/pnas.1900278116

Magney, T. S., Eitel, J. U. H., Huggins, D. R., & Vierling, L. A. (2016). Proximal NDVI derived phenology improves in-season predictions of wheat quantity and quality. *Agricultural and Forest Meteorology*, *217*, 46–60. https://doi.org/10.1016/j.agrformet.2015.11.009

Mäkelä, A., Hari, P., Berninger, F., Hänninen, H., & Nikinmaa, E. (2004). Acclimation of photosynthetic capacity in Scots pine to the annual cycle of temperature. *Tree Physiology*, *24*(4), 369–376. https://doi.org/10.1093/treephys/24.4.369

Maxwell, K., & Johnson, G. N. (2000). Chlorophyll fluorescence—A practical guide. *Journal of Experimental Botany*, *51*(345), 659–668. https://doi.org/10.1093/jexbot/51.345.659

Melaas, E. K., Sulla-Menashe, D., Gray, J. M., Black, T. A., Morin, T. H., Richardson, A. D., & Friedl, M. A. (2016). Multisite analysis of land surface phenology in North American temperate and boreal deciduous forests from Landsat. *Remote Sensing of Environment*, *186*, 452–464. https://doi.org/10.1016/j.rse.2016.09.014

Míguez, F., Fernández-Marín, B., Becerril, J. M., & García-Plazaola, J. I. (2015). Activation of photoprotective winter photoinhibition in plants from different environments: A literature compilation and meta-analysis. *Physiologia Plantarum*, *155*(4), 414–423. https://doi.org/10.1111/ppl.12329

Monson, R. K., Turnipseed, A. A., Sparks, J. P., Harley, P. C., Scott-Denton, L. E., Sparks, K., & Huxman, T. E. (2002). Carbon sequestration in a high-elevation, subalpine forest. *Global Change Biology*, *8*(5), 459–478. https://doi.org/10.1046/j.1365-2486.2002.00480.x

Muggeo, V. M. R. (2003). Estimating regression models with unknown break-points. *Statistics in Medicine*, *22*, 3055–3071.

Muggeo, V.M.R., 2008. Segmented: An R package to fit regression models with broken-line relationships. R News 8/1, 20-25, URL http://cran.r-project.org/doc/Rnews/

Norton, A. J., Rayner, P. J., Koffi, E. N., Scholze, M., Silver, J. D., & Wang, Y.-P. (2018). Estimating global gross primary productivity using chlorophyll fluorescence and a data assimilation system with the BETHY-SCOPE model. *Biogeosciences Discussions*, 1–40. https://doi.org/10.5194/bg-2018-270

Oleson, K.W., Lawrence, D.M., Bonan, G.B., Drewniak, B., Huang, M., Koven, C.D., et al. (2013). Technical description of version 4.5 of the Community Land Model (CLM). Retrieved from http://www.cesm.ucar.edu/models/cesm1.2/clm/CLM45_Tech_Note.pdf

Porcar-Castell, A. (2011). A high-resolution portrait of the annual dynamics of photochemical and non-photochemical quenching in needles of *Pinus sylvestris*. *Physiologia Plantarum*, *143*(2), 139–153. https://doi.org/10.1111/j.1399-3054.2011.01488.x

Porcar-Castell, A., Garcia-Plazaola, J. I., Nichol, C. J., Kolari, P., Olascoaga, B., Kuusinen, N., et al. (2012). Physiology of the seasonal relationship between the photochemical reflectance index and photosynthetic light use efficiency. *Oecologia*, *170*(2), 313–323. https://doi.org/10.1007/s00442-012-2317-9

Porcar-Castell, A., Pfündel, E., Korhonen, J. F. J., & Juurola, E. (2008). A new monitoring PAM fluorometer (MONI-PAM) to study the short- and long-term acclimation of photosystem II in field conditions. *Photosynthesis Research*, *96*(2), 173–179. https://doi.org/10.1007/s11120-008-9292-3

Porcar-Castell, A., Tyystjärvi, E., Atherton, J., van der Tol, C., Flexas, J., Pfündel, E. E., et al. (2014). Linking chlorophyll a fluorescence to photosynthesis for remote sensing applications: Mechanisms and challenges. *Journal of Experimental Botany*, *65*(15), 4065–4095. https://doi.org/10.1093/jxb/eru191

R Development Core Team, 2018. R: A language and environment for statistical computing. R Foundation for Statistical Computing, Vienna, Austria, URL https://www.R-project.org

Raczka, B., Duarte, H. F., Koven, C. D., Ricciuto, D., Thornton, P. E., Lin, J. C., & Bowling, D. R. (2016). An observational constraint on stomatal function in forests: Evaluating coupled carbon and water vapor exchange with carbon isotopes in the Community Land Model (CLM4.5). *Biogeosciences*, *13*(18), 5183–5204. https://doi.org/10.5194/bg-13-5183-2016

Reick, C. H., Raddatz, T., Brovkin, V., & Gayler, V. (2013). Representation of natural and anthropogenic land cover change in MPI-ESM. *Journal of Advances in Modeling Earth Systems*, *5*, 459–482. https://doi.org/10.1002/jame.20022

Richardson, A. D., Hufkens, K., Milliman, T., Aubrecht, D. M., Furze, M. E., Seyednasrollah, B., et al. (2018). Ecosystem warming extends vegetation activity but heightens vulnerability to cold temperatures. *Nature*, *560*(7718), 368–371. https://doi.org/10.1038/s41586-018-0399-1

Rocca, M. E., Brown, P. M., MacDonald, L. H., & Carrico, C. M. (2014). Climate change impacts on fire regimes and key ecosystem services in Rocky Mountain forests. *Forest Ecology and Management*, *327*, 290–305. https://doi.org/10.1016/j.foreco.2014.04.005

Schimel, D. T., Kittel, G. F., Running, S., Monson, R., Turnispeed, A., & Anderson, D. (2002). Carbon sequestration studied in western U.S. mountains. *Eos Trans. AGU*, *83*(40), 445–449. https://doi.org/10.1029/2002EO000314

Sun, J., Oncley, S. P., Burns, S. P., Stephens, B. B., Lenschow, D. H., Campos, T., et al. (2010). A multiscale and multidisciplinary investigation of ecosystem-atmosphere CO_2 exchange over the rocky mountains of Colorado. *Bulletin of the American Meteorological Society*, *91*(2), 209–230. https://doi.org/10.1175/2009BAMS2733.1

Sun, Y., Frankenberg, C., Wood, J. D., Schimel, D. S., Jung, M., Guanter, L., et al. (2017). OCO-2 advances photosynthesis observation from space via solar-induced chlorophyll fluorescence. *Science*, *358*(6360), eaam5747. https://doi.org/10.1126/science.aam5747

Thum, T., Zaehle, S., Köhler, P., Aalto, T., Aurela, M., Guanter, L., et al. (2017). Modelling sun-induced fluorescence and photosynthesis with a land surface model at local and regional scales in northern Europe. *Biogeosciences*, *14*(7), 1969–1987. https://doi.org/10.5194/bg-14-1969-2017

van der Tol, C., Berry, J. A., Campbell, P. K. E., & Rascher, U. (2014). Models of fluorescence and photosynthesis for interpreting measurements of solar-induced chlorophyll fluorescence. *Journal of Geophysical Research: Biogeosciences*, *119*, 2014JG002713. https://doi.org/10.1002/2014JG002713

van der Tol, C., Verhoef, W., & Rosema, A. (2009). A model for chlorophyll fluorescence and photosynthesis at leaf scale. *Agricultural and Forest Meteorology*, *149*(1), 96–105. https://doi.org/10.1016/j.agrformet.2008.07.007

Verhoeven, A. (2014). Sustained energy dissipation in winter evergreens. *New Phytologist*, *201*(1), 57–65. https://doi.org/10.1111/nph.12466

Walther, S., Voigt, M., Thum, T., Gonsamo, A., Zhang, Y., Köhler, P., et al. (2016). Satellite chlorophyll fluorescence measurements reveal large-scale decoupling of photosynthesis and greenness dynamics in boreal evergreen forests. *Global Change Biology*, *22*(9), 2979–2996. https://doi.org/10.1111/gcb.13200

Way, D. A., & Montgomery, R. A. (2015). Photoperiod constraints on tree phenology, performance and migration in a warming world. *Plant, Cell & Environment*, *38*(9), 1725–1736. https://doi.org/10.1111/pce.12431

Williams, C. A., Gu, H., MacLean, R., Masek, J. G., & Collatz, G. J. (2016). Disturbance and the carbon balance of US forests: A quantitative review of impacts from harvests, fires, insects, and droughts. *Global and Planetary Change*, *143*, 66–80. https://doi.org/10.1016/j.gloplacha.2016.06.002

Wong, C. Y. S., & Gamon, J. A. (2015). The photochemical reflectance index provides an optical indicator of spring photosynthetic activation in evergreen conifers. *New Phytologist*, *206*(1), 196–208. https://doi.org/10.1111/nph.13251

Yang, K., Ryu, Y., Dechant, B., Berry, J. A., Hwang, Y., Jiang, C., et al. (2018). Sun-induced chlorophyll fluorescence is more strongly related to absorbed light than to photosynthesis at half-hourly resolution in a rice paddy. *Remote Sensing of Environment*, *216*, 658–673. https://doi.org/10.1016/j.rse.2018.07.008

Yang, X., Tang, J., Mustard, J. F., Lee, J.-E., Rossini, M., Joiner, J., et al. (2015). Solar-induced chlorophyll fluorescence that correlates with canopy photosynthesis on diurnal and seasonal scales in a temperate deciduous forest. *Geophysical Research Letters*, *42*, 2015GL063201. https://doi.org/10.1002/2015GL063201

Zuromski, L. M., Bowling, D. R., Köhler, P., Frankenberg, C., Goulden, M. L., Blanken, P. D., & Lin, J. C. (2018). Solar-induced fluorescence detects interannual variation in gross primary production of coniferous forests in the Western United States. *Geophysical Research Letters.*, *45*(14), 7184–7193. https://doi.org/10.1029/2018GL077906